Engineered kinase activation reveals unique morphodynamic phenotypes and associated trafficking for Src family isoforms

Pei-Hsuan Chu[a,1], Denis Tsygankov[a,1], Matthew E. Berginski[b], Onur Dagliyan[a,c], Shawn M. Gomez[b], Timothy C. Elston[a], Andrei V. Karginov[a,2,3], and Klaus M. Hahn[a,d,3]

[a]Department of Pharmacology, [b]Department of Biomedical Engineering, [c]Department of Biochemistry and Biophysics, and [d]Lineberger Cancer Center, University of North Carolina at Chapel Hill, Chapel Hill, NC 27599

Edited by Stephen J. Benkovic, The Pennsylvania State University, University Park, PA, and approved July 16, 2014 (received for review March 11, 2014)

The Src kinase family comprises nine homologous members whose distinct expression patterns and cellular distributions indicate that they have unique roles. These roles have not been determined because genetic manipulation has not produced clearly distinct phenotypes, and the kinases' homology complicates generation of specific inhibitors. Through insertion of a modified FK506 binding protein (insertable FKBP12, iFKBP) into the protein kinase isoforms Fyn, Src, Lyn, and Yes, we engineered kinase analogs that can be activated within minutes in living cells (RapR analogs). Combining our RapR analogs with computational tools for quantifying and characterizing cellular dynamics, we demonstrate that Src family isoforms produce very different phenotypes, encompassing cell spreading, polarized motility, and production of long, thin cell extensions. Activation of Src and Fyn led to patterns of kinase translocation that correlated with morphological changes in temporally distinct stages. Phenotypes were dependent on N-terminal acylation, not on Src homology 3 (SH3) and Src homology 2 (SH2) domains, and correlated with movement between a perinuclear compartment, adhesions, and the plasma membrane.

image analysis | motion classification | live cell imaging | protein engineering | rapamycin

Since its discovery, c-Src (1) has been subject to intensive research into its cellular functions and regulation. Whereas c-Src is the best-studied protooncogene, less is known about the other, closely related Src family kinase (SFK) members. Their high degree of similarity in structure and regulation suggests that SFKs can partially compensate for each other in vivo. Indeed, knockout studies have shown that only mice deficient in all three genes (*src*, *yes*, and *fyn*) show embryonic lethality (2). Early studies demonstrated that disruption of Src or Fyn genes individually resulted only in subtle changes in function of a few cell types (e.g., osteoclasts for $src^{-/-}$, and T cells for $fyn^{-/-}$) (3, 4). Roche et al. provided strong evidence that Src, Yes, and Fyn substitute for each other during cell cycle progression (5). These studies suggested that there is a high degree of functional redundancy among Src family kinases.

Nonetheless, emerging evidence indicates that Src and Fyn regulate distinct processes in the same cell. Down-regulation of Fyn expression enhances VEGF-stimulated migration of endothelial cells, whereas down-regulation of Src does not (6). Differences in the transforming capacity of SFKs are thought to depend on their affinity for cholesterol-enriched membrane microdomains, which is determined in part by their N-terminal lipid modifications (7, 8). Src has higher tumorigenic potential than Fyn in prostate epithelium, and this is differently affected by alterations in N-terminal palmitoylation (9). Previous studies have shown that Src localizes to perinuclear endosomal compartments and translocates to the plasma membrane upon activation (10–12), whereas Fyn localizes to the plasma membrane regardless of its activity (13, 14). Although these studies suggest that localization is important in differentiating the actions of the two kinases, they do not identify specific roles associated with particular subcellular locations.

Various techniques have been applied to elucidate the differences in signaling specificity of SFKs. Kinase–substrate interactions have been examined using purified substrates (15). Mutated kinases with selectivity for radiolabeled ATP analogs have identified directly phosphorylated substrates of Src (16). These methods were restricted to cell lysates or purified proteins, and so were unable to address the role of cellular localization in substrate specificity.

To dissect the unique role of different SFK isoforms (2–4, 17, 18) in living cells, we engineered regulatable analogs of Fyn, Yes, and LynA kinases using our rapamycin-regulated activation (RapR) strategy, which has been developed using Src as a prototype (19, 20). Insertable FKBP12 (iFKBP, a truncated form of FKBP) was inserted into the catalytic domain of each SFK, which abolished their kinase activity. Activity was rescued by treating cells with rapamycin in the presence of the FKBP12-rapamycin binding domain (FRB) (Fig. 1*A*). Molecular dynamics studies have indicated that heterodimerization of the inserted iFKBP with FRB likely reduces the conformational mobility of the kinase G loop, restoring ATP binding (3, 21).

These analogs enabled activation of each isoform specifically, within minutes, resulting in clear phenotypic differences. Unlike genetic modifications of cell populations, there was little time for the cell to compensate for kinase activation before observation.

Significance

Src family kinases (SFKs), critical in many aspects of homeostasis and disease, occur as multiple isoforms. It has been difficult to dissect the unique function of each isoform because their structures are so similar. Here we specifically activated each SFK isoform through insertion of an engineered domain. The domain caused the kinases to be catalytically inactive until they were reactivated by the small molecule rapamycin. Computational methods for quantifying dynamic changes in cell shape revealed that activation of each isoform produced dramatically different cell behaviors. Quantitative analysis showed that these behaviors correlated with specific patterns of subcellular trafficking, and depended on isoform acylation.

Author contributions: P.-H.C., D.T., O.D., A.V.K., and K.M.H. designed research; P.-H.C., D.T., O.D., and A.V.K. performed research; D.T., M.E.B., S.M.G., T.C.E., and A.V.K. contributed new reagents/analytic tools; P.-H.C., D.T., M.E.B., O.D., S.M.G., T.C.E., A.V.K., and K.M.H. analyzed data; and P.-H.C., D.T., O.D., T.C.E., A.V.K., and K.M.H. wrote the paper.

The authors declare no conflict of interest.

This article is a PNAS Direct Submission.

[1]P.-H.C. and D.T. contributed equally to this work.

[2]Present address: Department of Pharmacology, University of Illinois at Chicago, Chicago, IL 60612.

[3]To whom correspondence may be addressed. Email: khahn@med.unc.edu or karginov@uic.edu.

This article contains supporting information online at www.pnas.org/lookup/suppl/doi:10.1073/pnas.1404487111/-/DCSupplemental.

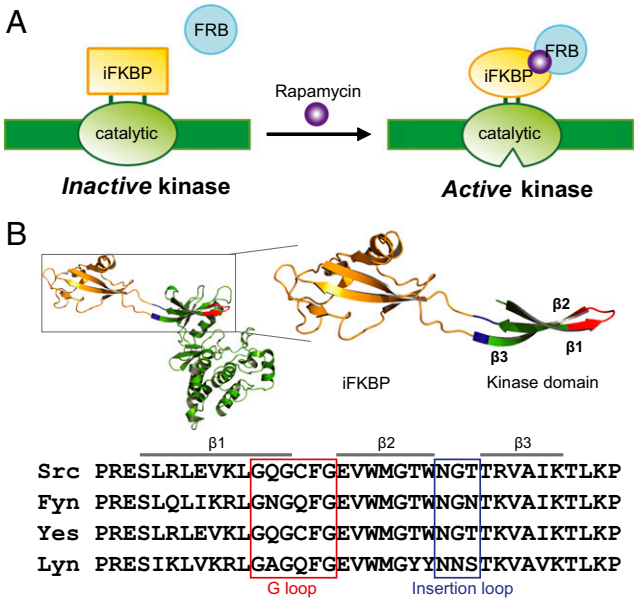

Fig. 1. Design of RapR kinases. (*A*) Schematic representation of the approach used to regulate catalytic activity of SFKs. The insertion of iFKBP at a highly conserved site in the catalytic domain of each kinase resulted in loss of kinase activity. Catalytic activity was restored by rapamycin, which induced binding of iFKBP and coexpressed FRB. (*B*) Sequence alignment of SFKs shows that there is a well-defined loop where iFKBP is inserted (blue). It is linked to the G loop (red) through a β-sheet in each SFK.

The induced cell behaviors occurred in a succession of stages, associated with changes in the subcellular distribution of each kinase. We focused on Src and Fyn, developing quantitative tools to carefully characterize the kinetics of induced behaviors and associated localization dynamics. Our results indicated that Src's unique ability to induce polarized movement shortly after kinase activation results from its localization in a perinuclear compartment, where it phosphorylates substrates that traffic on microtubules to the cell perimeter. Both the localization dynamics and phenotype differences between Src and Fyn were dependent on N-terminal lipid modifications, and not on SH2 and SH3 domain interactions.

Results

Based on the structural similarity of the catalytic domains in the SFKs (3, 21), we first identified the appropriate site for insertion of iFKBP into Fyn, Yes, and LynA. The insertion site could be identified simply through sequence analysis: iFKBP was inserted in a sequence linking the kinase G loop with a β-sheet in the catalytic domain (Fig. 1*B*). A constitutively activating mutation was included so that kinase activity would be solely under the control of rapamycin. To optimize the regulation of kinase activity, we tested various linkers connecting iFKBP to the catalytic domain of Fyn, using in vitro kinase assays. Whereas the shorter linkers gave similar results, the longest linker (GS_3PG–GPG) showed the weakest restoration of catalytic activity, suggesting that the longer linker could not propagate conformational changes to the G loop. Formation of the kinase–FRB complex, and resultant kinase activation, occurred only in the presence of rapamycin (Fig. S1*A*). Based on this optimization of the iFKBP insertion, we generated RapR Yes and RapR LynA using a short linker (GPG–GPG) to fuse iFKBP into the kinase catalytic domains (Fig. S1 *B* and *C*). Each of these RapR kinases showed restored activity upon treatment with rapamycin. Importantly, upon addition of rapamycin, catalytically inactive (kinase dead) mutants of the RapR kinases formed complexes with FRB but showed no change in activity, indicating that kinase activity was induced by rapamycin treatment (Fig. S1). RapR Fyn produced normal levels of phosphorylation for endogenous p130 Crk-associated substrate (p130Cas), focal adhesion kinase (FAK), cortactin, and paxillin (Fig. S2). Published characterization of RapR Src and its analogs indicated that it has normal kinetics, localization, and levels of kinase activity (19, 22, 23).

Because the RapR kinases enabled rapid and specific activation of each SFK, they could be used to examine the immediate effects of individual Src family members on cell behavior. Each RapR kinase was coexpressed with FRB in COS-7 cells and activated by adding rapamycin. Fig. 2*A* and Movies S1–S4 show the clearly distinct morphological changes produced by each isoform. Activation of Fyn generated uniform spreading, whereas activation of Src initiated polarized movement. LynA, which is mainly expressed in hematopoietic cells (24), induced long membrane projections with complex shapes, including sharp bends. Activation of Yes induced a phenotype intermediate between that of Src and Fyn.

We decided to focus on Fyn and Src because of their strongly contrasting phenotypes and their well-documented role in metastasis (25–27). To objectively analyze complex changes in cell morphology induced by each kinase required unbiased computational tools that could capture and quantify key features of cellular motion. To this end, we developed versatile methods for analyzing changes in cell shape and position. Our approach not only provides rigor in the comparison of experimental observations, but also enables the extraction of information that is not readily apparent by visual inspection. Here we provide a brief description of our methods: To characterize polarized movement, the inward or outward displacement of the cell edge was determined for each pair of successive time frames at points equally spaced along the edge. The displacements were mapped onto a circle and the degree of polarization in the displacement distribution was computed, enabling us to quantify consistently the polarized movement of cells with arbitrary geometry (Fig. 2*B*). As a second measure of shape changes, we calculated the change in cell area between successive time frames. An informative way to visualize these two parameters (polarization and rate of area change) is to plot them as points in 2D parameter space. In this way the data form a trajectory that shows the changing behavior of the cell over time (Fig. 2 *B* and *C* and Movie S5). Dividing the parameter space into distinct regions allowed us to classify cell shape changes for each time point as one of five different types of motion: uniform spreading, polarized spreading, polarized movement, polarized shrinkage, and uniform shrinkage. We used this method to compare cells in which either Fyn or Src had been activated. The plot in Fig. 2*D* (from 57 Fyn cells and 55 Src cells) shows the distributions for the five different cellular behaviors across the populations and how these distributions changed over time. Both Fyn and Src initially produced extensive spreading, but only for Src was this followed by polarized movement (see also Fig. S3 and Table S1). We were concerned that the differences between Fyn and Src might be due to differences in expression level, so we compared kinase expression in the flat COS-7 cells by determining the brightness per unit area of EGFP-tagged RapR kinases. Comparing high versus low expressers (Fig. S4) showed that expression level did not affect our conclusions. These studies quantified clear differences in the morphodynamic cell behaviors induced by Fyn versus Src.

We next sought to identify which structural features of Fyn and Src were responsible for their induction of different phenotypes. The SH3 and SH2 domains of SFKs have been identified as effector binding sites and were proposed to mediate signaling specificity (28–31). Surprisingly, switching the effector binding domains of Src and Fyn had little effect on the cellular responses described above (Fig. S5 *A*–*C*). There were, however, striking differences in the initial localization and localization dynamics of Fyn and Src. RapR kinases were labeled with EGFP to visualize their localization during activation (Movies S6 and S7), and kinetics of localization changes were quantified as shown in Fig. 3 *A* and *B*. Before activation, wild-type Src was concentrated on one side of the nucleus, where it has been shown to be associated with the Golgi apparatus and vesicular compartments (12, 14, 32). In contrast,

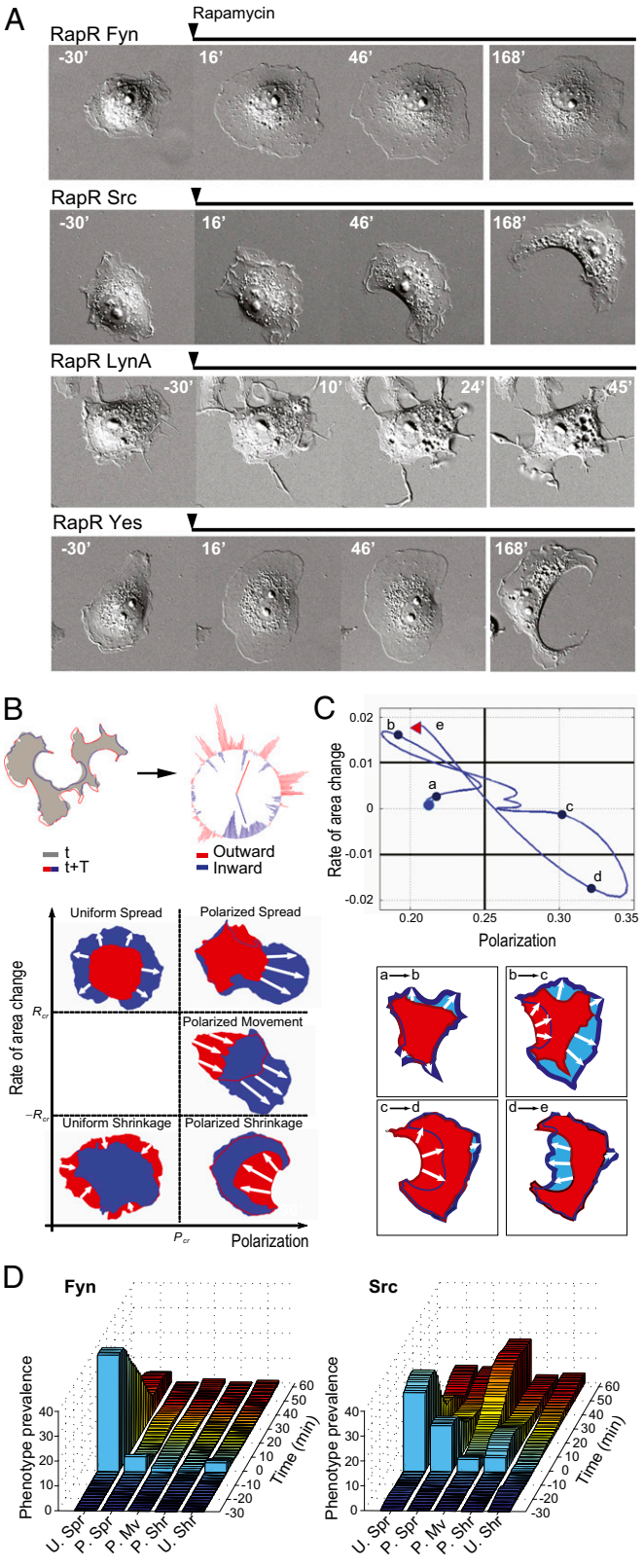

Fig. 2. Distinct morphological changes resulted from activating different SFK isoforms. (*A*) Morphological changes induced by activating different SFKs in COS-7 cells. (*B*) Automated cell analysis used to quantify morphological changes. (*Upper Left*) The gray area shows a cell at time t. Red and blue line segments show relative cell motion in the time interval T (outward motion red, inward motion blue). (*Upper Right*) The displacement of points equally spaced around the cell edge was mapped onto a circle to assess polarization. (*Lower*) A parameter space formed by the rate of area change and polarization is used to characterize boundary motion over time, with different regions of the parameter space corresponding to characteristic types of cell motion. (*C*) The morphodynamics of each cell was represented as a trajectory in parameter space. (*Lower*) Shape changes between two time points (early red, later blue) for a specific cell; (*Upper*) These transitions are noted. (*D*) The timing of specific morphological changes analyzed in populations of RapR Fyn versus RapR Src cells using this quantitative method. P. Mv, polarized movement; P. Shr, polarized shrinkage; P. Spr, polarized spreading; U. Shr, uniform shrinkage; U. Spr, uniform spreading.

wild-type Fyn showed uniform distribution in the plasma membrane (with some concentration in membrane patches and puncta, but no perinuclear accumulation) (Fig. 3*C* and Fig. S6). After addition of rapamycin, Src moved away from the perinuclear region as polarized movement began. Fyn remained uniformly distributed upon activation (Fig. 3*B*). Analyzing the kinetics of localization dynamics showed that Src's induction of polarized motility coincided with its departure from the perinuclear compartment (Figs. 2*D* and 3*B*). Swapping the SH3-SH2 domains of Src and Fyn did not affect their localization or translocation upon activation (Fig. S5*D*).

We examined acylation of Fyn and Src (Fig. 3*A*) because acylation is an important determinant of kinase distribution (8, 13, 33, 34). Both Fyn and Src are cotranslationally myristoylated at an N-terminal glycine, but only Fyn is palmitoylated, at cysteines 3 and 6 (33, 35). We used previously described mutations of the SH4 domain to alter the lipidation of the two proteins (14, 33) (Fig. 3*A*): In Fyn, Cys3 and Cys6 were substituted for serines to eliminate the addition of palmitoyl groups (Fyn Palm$^-$), rendering the acylation of Fyn like that of Src (33). To render the acylation of Src like that of Fyn, serines 3 and 6 were substituted with cysteines, generating the Fyn acylation pattern (Src Palm$^+$). Remarkably, removal of the palmitoylation sites from Fyn (Fyn Palm$^-$) resulted in conversion to the Src phenotype (Figs. 3*B* and 4 *A* and *B*, *Left*), producing kinase accumulation at the perinuclear region before activation, kinase dispersion upon activation, and induction of polarized movement. In contrast, introducing cysteine into Src (Src Palm$^+$) did not produce clear conversion to a Fyn phenotype (Fig. 4*B*, *Right*). Src Palm$^+$ continued to show perinuclear localization before activation, and dispersion upon activation (Fig. 3*B*). Cells did show a reduction in the persistence of polarized movement produced by wild-type Src (Fig. S7*C*). Conversion of Fyn localization and trafficking patterns to those of Src were accompanied by conversion to the Src motility phenotype. This strongly suggests that perinuclear localization and translocation from the perinuclear region is important to Src's unique ability to induce polarized movement (Fig. 3*B*). Simply adding palmitoylatable cysteines to Src was not sufficient to produce Fyn phenotypes or trafficking patterns. This could be because palmitoylation was incomplete [as previously observed (33)], or because Src possesses additional sequences that are involved in anchoring at the perinuclear region.

Signaling messengers travel along microtubules to specific regions of the cell edge to produce polarization (36–39), so we examined whether microtubules (MT) are required for Src-induced polarized movement. Cells were treated with the MT polymerization inhibitor nocodazole before addition of rapamycin. Upon kinase activation, nocodazole-treated cells protruded randomly rather than undergoing directed motility (Fig. 5*A* and Movie S8), consistent with a role for MT in regulation of cell polarization (39). Interestingly, Src release from the perinuclear compartment occurred despite MT disruption, indicating that release was under the control of a mechanism independent of trafficking on MT, consistent with previous studies (10).

We examined the role of Src's Unique domain, a non-conserved region within SFKs that is thought to mediate SFK–lipid interactions (40, 41). Replacing the Unique domain of Src with that of Fyn [Src(FynSH4U)] reduced but did not fully abrogate the perinuclear localization of Src. Upon activation, the

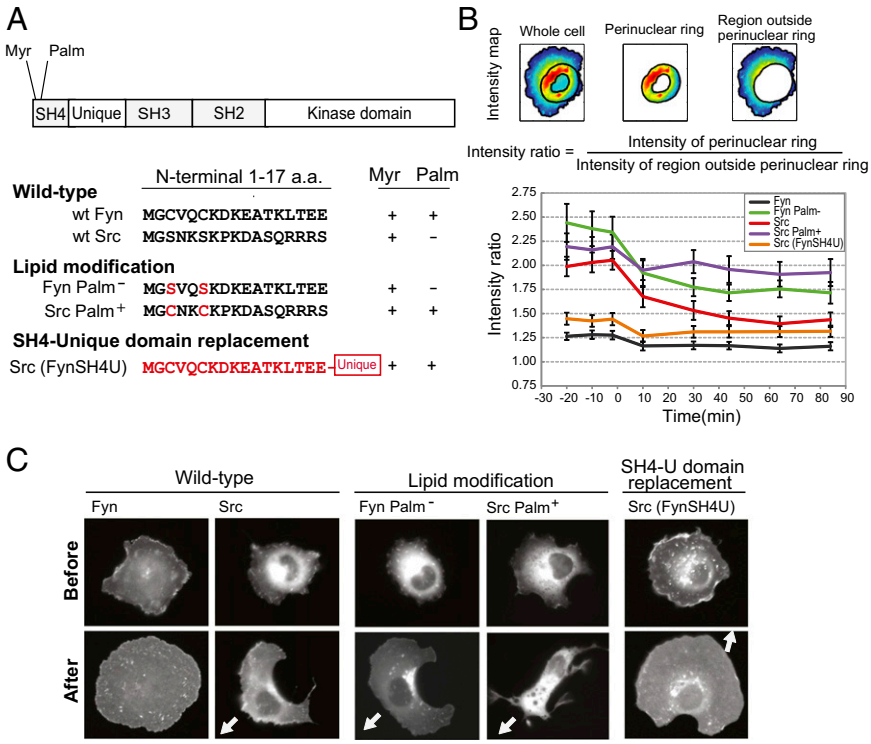

Fig. 3. Modifying the N terminus of Src and Fyn resulted in different cellular distributions and translocations, with corresponding changes in kinase-induced morphodynamics. (*A*) Nomenclature of Fyn and Src constructs used in this study. Changes in amino acids and protein domains are labeled in red. (*B*) Kinase distribution was quantified as the ratio of fluorescence intensities in a region of 10 μm from the nucleus and in the remainder of the cell. Error bars indicate 90% confidence intervals ($n > 55$ cells). Kinases were activated at time 0. The relatively high initial values and decreasing ratio over time indicated that Fyn Palm$^-$, Src, and Src Palm$^+$ were initially localized at the perinuclear region and dispersed upon activation. The cellular distribution of Fyn and Src(FynSH4U) was more diffuse both before and after activation. (*C*) Representative fluorescent images of COS-7 cells expressing Fyn, Src, and their derivatives show the subcellular localization of kinases before and after activation, as cells undergo morphological changes. Arrows indicate direction of movement.

Src–Fyn chimera again dispersed, leading to clear but delayed polarized movement (Figs. 3 and 4*C*).

SFKs are known to mediate adhesion signaling in motility (42, 43), and both Fyn and Src affected focal adhesions upon activation (Movies S9 and S10). Because adhesion changes were too complex to characterize by eye, we turned to our recently published methods for quantitative analysis of adhesion dynamics (44). Both Src and Fyn increased adhesion turnover, but Src had a stronger effect. Accumulation at adhesions was seen for RapR Src but not RapR Fyn. The removal of Fyn's palmitoyl groups (Fyn Palm−), which had caused it to duplicate Src's trafficking patterns, also increased its accumulation at adhesions (Figs. 3*B* and 5*B*). Src's induction of disassembly may be important to its induction of polarized motility, as translocating cells must detach their trailing edges.

Discussion

RapR analogs provided rapid activation of specific SFK isoforms in living cells, revealing distinct phenotypes induced by Fyn, Src, Yes, and Lyn. Striking differences indicated a unique role for each isoform in the control of morphodynamics. To quantify and characterize the role of each isoform in regulating cellular dynamics, we developed a suite of computational tools that could analyze the distribution of behaviors across cell populations. These tools revealed that Fyn and Src initially generated symmetric spreading, but only Src produced polarized cell movement at later times. The different phenotypes induced by Src and Fyn were associated with distinct trafficking patterns: Src produced polarized spreading only after it was released from a perinuclear compartment, when it moved to the plasma membrane and focal adhesions, inducing increased adhesion turnover. Fyn was distributed more uniformly both before and after activation, and generated uniform cell spreading. Effects of nocodazole were consistent with a role for MT-mediated trafficking in producing polarization, but MTs were not required for Src release from the perinuclear compartment. Trafficking and phenotypes were strongly dependent on N-terminal acylation, but not on the kinases' SH2 and SH3 interaction domains.

Both Src and Fyn initially triggered uniform, symmetric cell spreading. However, after this initial stage, only Src produced predominantly polarization and motility. These differences were not dictated by the SH3 or SH2 domains that play important roles in Src and Fyn's substrate binding and subcellular targeting (17, 18). Rather, the distinct lipid modifications of each kinase played an important role in both these phenotypes and in localization dynamics. Stimulation of polarized movement required activation-dependent translocation of Src from a perinuclear compartment to the plasma membrane. A prevailing hypothesis regarding Src's induction of polarization, derived from studies of Src activation by integrins and growth factor receptors, is that Src is activated at specific regions of the plasma membrane to produced localized protrusions and thereby drive polarized movement (3, 45, 46). However, our observations suggest that polarized migration can be initiated by activation of Src at a perinuclear compartment. This raises two possibilities: either activated Src is translocated to specific locations at the plasma membrane, where it produces protrusion and migration, or Src phosphorylates proteins in the perinuclear compartment, and these proteins are then transported to locations at the cell periphery. We were unable to identify any asymmetry of RapR Src localization when it moved to the plasma membrane. Furthermore, our data indicated that activated Src translocated to the plasma membrane independently of MT, but Src-mediated polarization of cells required an intact MT network. Thus, it is most likely that MT are responsible for targeted delivery of Src substrates that are initially phosphorylated by Src at the perinuclear compartment.

This hypothesis is also consistent with our results showing that RapR Src can stimulate polarized cell migration even when its N-terminal portion has been substituted with the N-terminal SH4-Unique domain of Fyn. This modification reduces the perinuclear localization of inactive RapR Src normally seen before activation, but a noticeable fraction still remains at the perinuclear region. The reduced amount of RapR Src is apparently still sufficient to phosphorylate the substrates in the perinuclear compartment, and thereby induce polarized migration.

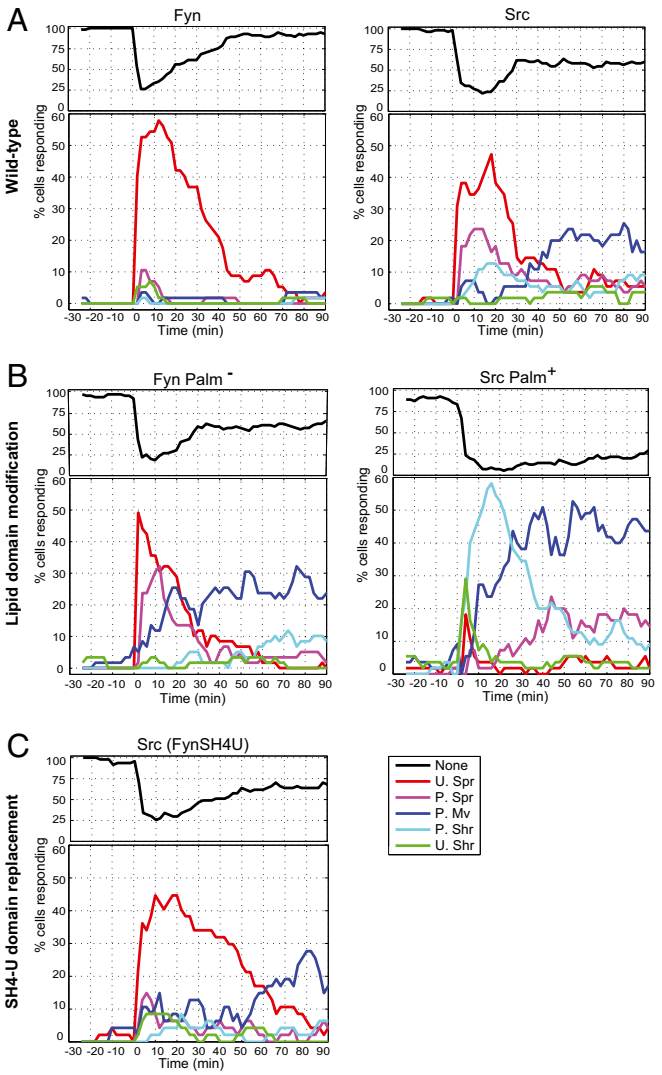

Fig. 4. Morphological changes induced by kinase activation. Graphs show the percentage of cells undergoing each behavior quantified as described in Fig. 2 *B* and *C*. Rapamycin was added at time 0. The upper part of each graph shows the percentage of cells that showed no response (black). P. Mv, P. Spr, P. Shr, U. Shr, and U. Spr are defined as in Fig. 2*D*.

However, the reduced levels of perinuclear Src led to delays in the migratory response (Fig. 4*C*).

Simply changing the N-terminal lipidation of Fyn to that of Src was sufficient to localize Fyn to the perinuclear compartment, and also enabled Fyn to generate the Src-specific phenotype. This, together with the fact that SH2 and SH3 substitutions had little effect on the differences between Fyn and Src, suggests that localization controls the substrate interactions and/or substrate interaction kinetics that produce differences between Src and Fyn.

In summary, rapid activation of the kinases made it possible to follow transient events they induced. In contrast, genetic manipulations generate changes over hours, altering protein expression rather than activation, and produce changes with widely differing rates across cell populations (Fig. S8). Although several studies have reported differences in the localization and trafficking of individual SFKs, this study presents direct evidence that distinct localizations of SFK are responsible for inducing different cellular responses, and sheds light on the role of trafficking in induction of polarization by Src. Because the site of iFKBP insertion in RapR kinases is highly conserved (19, 20, 23), the approach can likely be used to dissect the role of many kinases. Recent extensions include combining iFKBP and FRB into a single insertable domain, and directing the activated kinase to interact with a single, specific substrate (22, 23).

Materials and Methods

Generation of Src- and Fyn-Derived RapR Kinases. The Fyn Palm$^+$ (C3SC6S mutant Fyn) and Src Palm$^-$ (S3CS6C mutant Src) constructs were generated using the modified site-directed mutagenesis method described in *SI Materials and Methods*. The Src(FynSH4U) was prepared by replacing the SH4 and Unique domains of Src (aa 1–82) with those of Fyn (aa 1–81). To generate Src(FynSH32) and Fyn(SrcSH32), overlap extension PCR was used to generate the SrcSH3SH2 domain (Gly83 to Cys253) or the FynSH3SH2 domain (Thr82 to Cys246) and these were inserted into the corresponding site of RapR Fyn or RapR Src, to replace their original domains.

Live Cell Imaging. For cell morphology studies, COS-7 cells expressing EGFP-tagged RapR kinases and mCherry-tagged FRB were used. Cells were plated on fibronectin-coated coverslips (5 ug/mL fibronectin) 2 h before the experiment, then transferred to L-15 medium (Invitrogen) supplemented with 5% (vol/vol) FBS. Rapamycin was added into the medium 30 min after imaging. Live cell imaging was performed in a heated chamber using an Olympus IX-81 microscope equipped with an UPlanFLN 40× objective (Oil, N.A. 1.30). Image analysis was performed using Metamorph and MATLAB software. For focal adhesion studies, COS-7 cells expressing CFP-tagged RapR kinase, mCherry-tagged FRB, and mVenus-tagged vinculin were used. Live cell imaging was performed using an Olympus IX-81 microscope equipped with an objective-based total internal reflection fluorescence (TIRF) system and a PlanApo N 60× TIRF objective (N.A. 1.45). Time-lapse movies were taken at 2-min time intervals. All images were collected using a Photometrics CoolSnap ES CCD camera.

Quantification of Morphological Changes. All morphometric quantities were computed from fluorescence intensities generated by imaging COS-7 cells expressing EGFP-tagged RapR kinases. The analysis was performed using custom software written in MATLAB and specifically designed for this project. All software modules include a Graphical User Interface (GUI) for easy use. Image analysis involves two steps. The first step is cell boundary detection using the *MovThresh* module, which automatically determines an intensity threshold for each time frame of the movie. The GUI also provides options

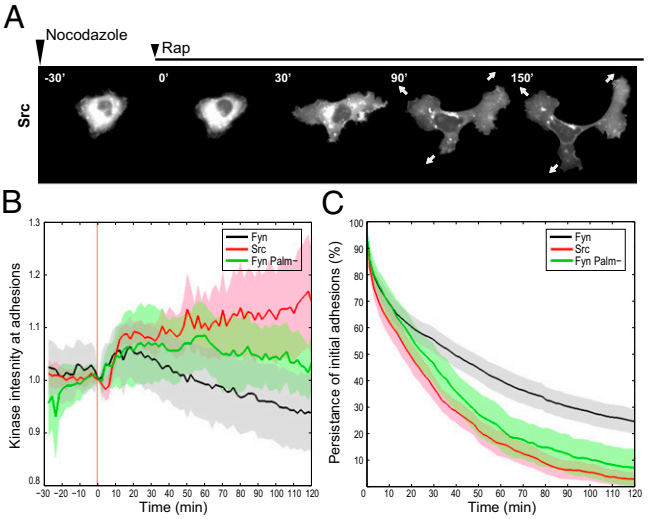

Fig. 5. Induction of polarized movement is dependent on translocation dynamics. (*A*) COS-7 cells treated with 10 μM nocodazole 30 min before Src activation showed multiple protrusions extending with no clear polarization. (*B*) Normalized mean kinase intensity at adhesions over time (shaded region indicates 95% confidence interval). The vertical red line indicates time of rapamycin treatment. ($n > 15$ cells from two independent experiments). (*C*) The persistence of adhesions, plotted as the percent initial intensity of mVenus-tagged vinculin remaining in adhesions over time (shaded regions show 95% confidence intervals, intensity at time of rapamycin addition = 100%).

that allow manual adjustment of the threshold value as needed. The second step is motion classification using the *Squigglymorph* module. This module finds and displays regions of protrusion and retraction using pairwise comparisons of cell boundary points at times t and $t+T$, where T is a user-defined time lag. The distribution of protruding boundary points is visualized by mapping the cell boundary to a circle, and boundary movements are quantified using the polarization vector, $\vec{p}(t)$, according to the equation

$$\vec{p}(t) = (p_x, p_y) = \left(\int_0^{2\pi} l(a)\cos(a)\mathrm{d}a, \int_0^{2\pi} l(a)\sin(a)\mathrm{d}a \right),$$

where a is the angular coordinate of the boundary point on the circle and $l(a)$ is the corresponding displacement of the boundary point between time t and $t+T$. For the polarization index,

$$P(t) = \sqrt{\langle p_x \rangle^2 + \langle p_y \rangle^2},$$

we use a running average of three polarization vectors from consecutive time points, which accounts for the persistence of the polarization. The polarization index and the rate of area change, $R(t) = \mathrm{d}A/\mathrm{d}t$, form a phase space that divides cell movement into six regions: (*i*) uniform spreading ($P < P_{cr}$, $R > R_{cr}$), (*ii*) polarized spreading ($P \geq P_{cr}$, $R > R_{cr}$), (*iii*) uniform shrinkage ($P < P_{cr}$, $R < -R_{cr}$), (*iv*) polarized shrinkage ($P \geq P_{cr}$, $R < -R_{cr}$), (*v*) polarized movement ($P \geq P_{cr}$, $|R| \leq R_{cr}$), and (*vi*) steady state ($P < P_{cr}$, $|R| \leq R_{cr}$). At each time point the cell is characterized as being in one of the six possible modes of motion and the dynamic behavior of the cell is visualized as a trajectory moves through phase space. The parameters P_{cr} and R_{cr} were adjusted to achieve good correspondence between the visually observed behavior and output from the analysis. For the analyses presented here the values of P_{cr} and R_{cr} were taken to be 0.28 and 0.005, respectively. The analysis results for individual cells ($n > 55$ for each construct) were then used to perform statistical analysis. Additional features of *Squigglymorph* include: (*i*) construction of smoothed curves for the parameters $P(t)$ and $R(t)$ using a user-defined smoothing window, and (*ii*) calculation of the mean-squared displacement (MSD) of the centroids and fitting the resulting curve to a persistent random walk to compute an estimate for the centroid speed and persistence (47, 48):

$$\mathrm{MSD} = \langle d^2(t) \rangle = 2S^2P\left[t - P\left(1 - e^{-t/P}\right)\right].$$

The directional persistence time P was obtained by MSD analysis of time-lapse movies of over 180 min in length.

Antibodies and reagents, cell culture, immunoprecipitation and kinase assays, cloning procedures, and focal adhesion imaging are described in *SI Materials and Methods*.

ACKNOWLEDGMENTS. We are grateful to Betsy Clarke and Marie Rougie for expert assistance in graphics and microscopy, Elena Fenu for preparation of constructs, and Dan Marston for critical reading of the manuscript. We thank the National Institutes of Health for funding (GM102924 to K.M.H., U01GM094663 to S.M.G., GMO79271 to T.C.E., and R21CA159179 to A.V.K.). O.D. is a Howard Hughes Medical Institute International Student Research Fellow.

1. Stehelin D, Varmus HE, Bishop JM, Vogt PK (1976) DNA related to the transforming gene(s) of avian sarcoma viruses is present in normal avian DNA. *Nature* 260(5547): 170–173.
2. Stein PL, Vogel H, Soriano P (1994) Combined deficiencies of Src, Fyn, and Yes tyrosine kinases in mutant mice. *Genes Dev* 8(17):1999–2007.
3. Thomas SM, Brugge JS (1997) Cellular functions regulated by Src family kinases. *Annu Rev Cell Dev Biol* 13:513–609.
4. Lowell CA, Soriano P (1996) Knockouts of Src-family kinases: Stiff bones, wimpy T cells, and bad memories. *Genes Dev* 10(15):1845–1857.
5. Roche S, Fumagalli S, Courtneidge SA (1995) Requirement for Src family protein tyrosine kinases in G2 for fibroblast cell division. *Science* 269(5230):1567–1569.
6. Werdich XQ, Penn JS (2005) Src, Fyn and Yes play differential roles in VEGF-mediated endothelial cell events. *Angiogenesis* 8(4):315–326.
7. Oneyama C, et al. (2009) Transforming potential of Src family kinases is limited by the cholesterol-enriched membrane microdomain. *Mol Cell Biol* 29(24):6462–6472.
8. Resh MD (1994) Myristylation and palmitylation of Src family members: The fats of the matter. *Cell* 76(3):411–413.
9. Cai H, et al. (2011) Differential transformation capacity of Src family kinases during the initiation of prostate cancer. *Proc Natl Acad Sci USA* 108(16):6579–6584.
10. Fincham VJ, et al. (1996) Translocation of Src kinase to the cell periphery is mediated by the actin cytoskeleton under the control of the Rho family of small G proteins. *J Cell Biol* 135(6 Pt 1):1551–1564.
11. Sandilands E, et al. (2004) RhoB and actin polymerization coordinate Src activation with endosome-mediated delivery to the membrane. *Dev Cell* 7(6):855–869.
12. Kasahara K, et al. (2007) Rapid trafficking of c-Src, a non-palmitoylated Src-family kinase, between the plasma membrane and late endosomes/lysosomes. *Exp Cell Res* 313(12):2651–2666.
13. Sato I, et al. (2009) Differential trafficking of Src, Lyn, Yes and Fyn is specified by the state of palmitoylation in the SH4 domain. *J Cell Sci* 122(Pt 7):965–975.
14. Sandilands E, Brunton VG, Frame MC (2007) The membrane targeting and spatial activation of Src, Yes and Fyn is influenced by palmitoylation and distinct RhoB/RhoD endosome requirements. *J Cell Sci* 120(Pt 15):2555–2564.
15. Takeda H, et al. (2010) Comparative analysis of human SRC-family kinase substrate specificity in vitro. *J Proteome Res* 9(11):5982–5993.
16. Shah K, Shokat KM (2002) A chemical genetic screen for direct v-Src substrates reveals ordered assembly of a retrograde signaling pathway. *Chem Biol* 9(1):35–47.
17. Brown MT, Cooper JA (1996) Regulation, substrates and functions of Src. *Biochim Biophys Acta* 1287(2-3):121–149.
18. Thomas SM, Soriano P, Imamoto A (1995) Specific and redundant roles of Src and Fyn in organizing the cytoskeleton. *Nature* 376(6537):267–271.
19. Karginov AV, Ding F, Kota P, Dokholyan NV, Hahn KM (2010) Engineered allosteric activation of kinases in living cells. *Nat Biotechnol* 28(7):743–747.
20. Karginov AV, Hahn KM (2011) Allosteric activation of kinases: Design and application of RapR kinases. *Current Protocols in Cell Biology* (Wiley, New York) Chap 14, unit 13.
21. Roskoski R, Jr (2004) Src protein-tyrosine kinase structure and regulation. *Biochem Biophys Res Commun* 324(4):1155–1164.
22. Karginov AV, et al. (2014) Dissecting motility signaling through activation of specific Src-effector complexes. *Nat Chem Biol* 10(4):286–290.
23. Dagliyan O, et al. (2013) Rational design of a ligand-controlled protein conformational switch. *Proc Natl Acad Sci USA* 110(17):6800–6804.
24. Yamanashi Y, et al. (1989) Selective expression of a protein-tyrosine kinase, p56lyn, in hematopoietic cells and association with production of human T-cell lymphotropic virus type I. *Proc Natl Acad Sci USA* 86(17):6538–6542.
25. Frame MC (2002) Src in cancer: deregulation and consequences for cell behaviour. *Biochim Biophys Acta* 1602(2):114–130.
26. Summy JM, Gallick GE (2003) Src family kinases in tumor progression and metastasis. *Cancer Metastasis Rev* 22(4):337–358.
27. Chen ZY, et al. (2010) Roles of Fyn in pancreatic cancer metastasis. *J Gastroenterol Hepatol* 25(2):293–301.
28. Koch CA, Anderson D, Moran MF, Ellis C, Pawson T (1991) SH2 and SH3 domains: Elements that control interactions of cytoplasmic signaling proteins. *Science* 252(5006):668–674.
29. Songyang Z, Cantley LC (1995) Recognition and specificity in protein tyrosine kinase-mediated signalling. *Trends Biochem Sci* 20(11):470–475.
30. Weng Z, et al. (1994) Identification of Src, Fyn, and Lyn SH3-binding proteins: implications for a function of SH3 domains. *Mol Cell Biol* 14(7):4509–4521.
31. Summy JM, Guappone AC, Sudol M, Flynn DC (2000) The SH3 and SH2 domains are capable of directing specificity in protein interactions between the non-receptor tyrosine kinases cSrc and cYes. *Oncogene* 19(1):155–160.
32. Pulvirenti T, et al. (2008) A traffic-activated Golgi-based signalling circuit coordinates the secretory pathway. *Nat Cell Biol* 10(8):912–922.
33. Alland L, Peseckis SM, Atherton RE, Berthiaume L, Resh MD (1994) Dual myristylation and palmitylation of Src family member p59fyn affects subcellular localization. *J Biol Chem* 269(24):16701–16705.
34. Wolven A, Okamura H, Rosenblatt Y, Resh MD (1997) Palmitoylation of p59fyn is reversible and sufficient for plasma membrane association. *Mol Biol Cell* 8(6):1159–1173.
35. Koegl M, Zlatkine P, Ley SC, Courtneidge SA, Magee AI (1994) Palmitoylation of multiple Src-family kinases at a homologous N-terminal motif. *Biochem J* 303(Pt 3):749–753.
36. Wadsworth P (1999) Regional regulation of microtubule dynamics in polarized, motile cells. *Cell Motil Cytoskeleton* 42(1):48–59.
37. Lippincott-Schwartz J, Roberts TH, Hirschberg K (2000) Secretory protein trafficking and organelle dynamics in living cells. *Annu Rev Cell Dev Biol* 16:557–589.
38. Schmoranzer J, Kreitzer G, Simon SM (2003) Migrating fibroblasts perform polarized, microtubule-dependent exocytosis towards the leading edge. *J Cell Sci* 116(Pt 22): 4513–4519.
39. Etienne-Manneville S (2013) Microtubules in cell migration. *Annu Rev Cell Dev Biol* 29:471–499.
40. Summy JM, et al. (2003) The SH4-Unique-SH3-SH2 domains dictate specificity in signaling that differentiate c-Yes from c-Src. *J Cell Sci* 116(Pt 12):2585–2598.
41. Pérez Y, et al. (2013) Lipid binding by the Unique and SH3 domains of c-Src suggests a new regulatory mechanism. *Sci Rep* 3:1295.
42. Volberg T, Romer L, Zamir E, Geiger B (2001) pp60(c-src) and related tyrosine kinases: A role in the assembly and reorganization of matrix adhesions. *J Cell Sci* 114(Pt 12): 2279–2289.
43. Webb DJ, et al. (2004) FAK-Src signalling through paxillin, ERK and MLCK regulates adhesion disassembly. *Nat Cell Biol* 6(2):154–161.
44. Berginski ME, Vitriol EA, Hahn KM, Gomez SM (2011) High-resolution quantification of focal adhesion spatiotemporal dynamics in living cells. *PLoS ONE* 6(7):e22025.
45. Bromann PA, Korkaya H, Courtneidge SA (2004) The interplay between Src family kinases and receptor tyrosine kinases. *Oncogene* 23(48):7957–7968.
46. Playford MP, Schaller MD (2004) The interplay between Src and integrins in normal and tumor biology. *Oncogene* 23(48):7928–7946.
47. Dunn GA (1983) Characterising a kinesis response: Time averaged measures of cell speed and directional persistence. *Agents Actions Suppl* 12:14–33.
48. Othmer HG, Dunbar SR, Alt W (1988) Models of dispersal in biological systems. *J Math Biol* 26(3):263–298.